Molecularly-Sensitive Optical Ranging using Nonlinear Interferometric Vibrational Imaging

Daniel L. Marks[a,b], Claudio Vinegoni[a,b], Jeremy S. Bredfeldt[a,b], and Stephen A. Boppart[a,b,c]

[a]Electrical and Computer Engineering Department, University of Illinois at Urbana-Champaign, 1406 W. Green, Urbana IL 61801

[b]Beckman Institute for Advanced Science an Technology, University of Illinois at Urbana-Champaign, 405 N. Mathews, Urbana IL 61801

[c]Department of Bioengineering, College of Medicine, University of Illinois at Urbana-Champaign, Urbana IL 61801

ABSTRACT

We explore combining Coherent anti-Stokes Raman Scattering with Optical Coherence Tomography ranging when low numerical aperture scanning is used, and demonstrate ranging of layers in a Raman-active medium.

Keywords: Optical Coherence Tomography, Nonlinear Optics, Raman Spectroscopy

1. INTRODUCTION

Optical Coherence Tomography[1–4] has proved to be an enormously successful imaging modality for imaging at the 2-20 μm length scales. However, it is limited in applicability by the properties it measures, that is the linear scattering properties of samples. These linear properties can indicate the absorption,[5–7] refractive index,[8,9] scattering, and birefringence[10–13] of a sample, but do not encode the density of specific molecules. To overcome this, dyes and scattering contrast agents[14,15] can be used to mark targets of interest with detectable features. To avoid introducing foreign substances into biological tissues, exogenous properties such as Raman-active vibrations can be used. Coherent anti-Stokes Raman Scattering (CARS) microscopy[16–23] scans a tightly focused beam through tissue to produce a nonlinear Raman effect in a confined region. Incoherently detected CARS is unable to distinguish between photons emitted at various points inside the focal region, so the focal region must be small to achieve high resolution. Therefore to scan a large volume requires serially scanning many small focal volumes and a long scanning time.

In conventional OCT, features are distinguished within the focal volume by the time of arrival of the signal using interferometric detection. If a low NA objective is used, a large diameter beam is created with a larger depth-of-field. This enables OCT to scan a larger volume at a lower resolution, with the time of arrival used rather than a tight focus to distinguish depth. Because the anti-Stokes radiation in CARS is emitted coherently with respect to the pump and Stokes radiation, it too can be distinguished interferometrically by its time of

Inquiries should be directed to *boppart@uiuc.edu*, Telephone: 1-217-244-7479.

Coherence Domain Optical Methods and Optical Coherence Tomography in Biomedicine IX, edited by Valery V. Tuchin, Joseph A. Izatt, James G. Fujimoto, Proc. of SPIE Vol. 5690 (SPIE, Bellingham, WA, 2005) · 1605-7422/05/$15 · doi: 10.1117/12.592725

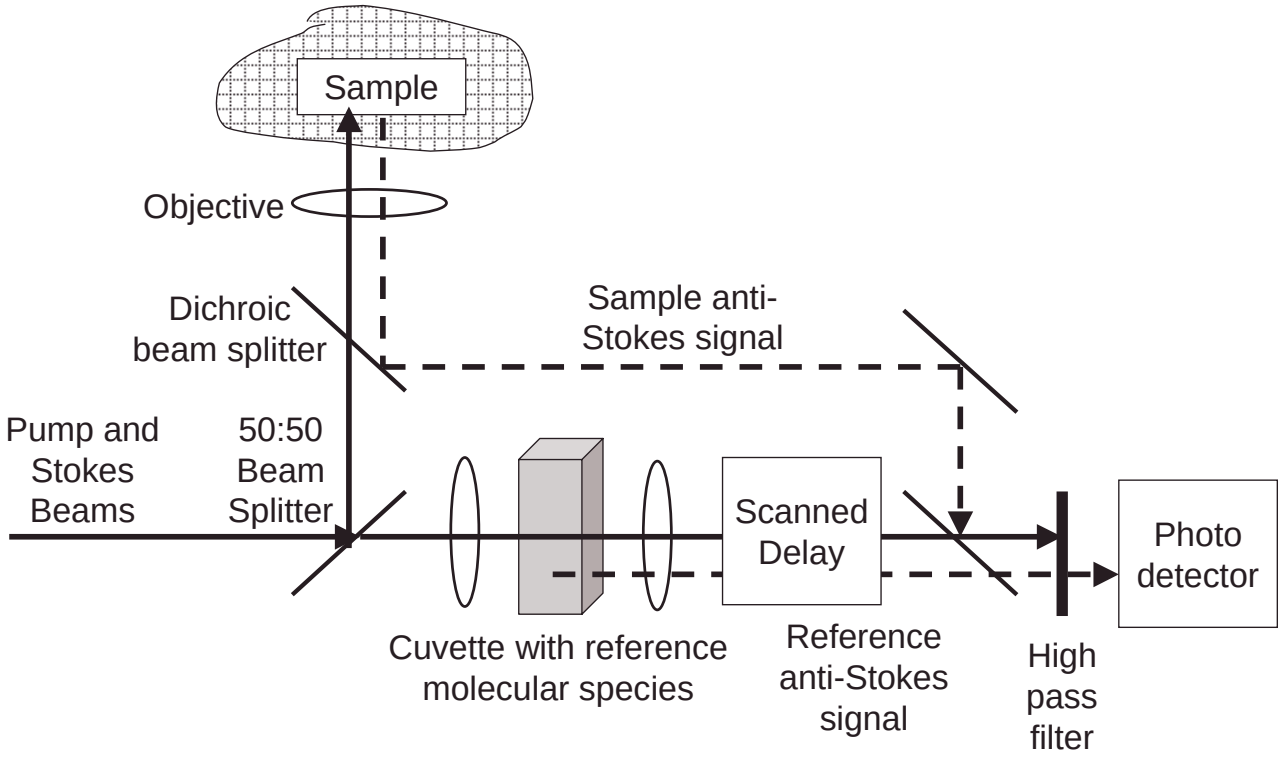

Figure 1. Prototype of setup used for CARS temporal ranging.

arrival, enabling this scanning mode to be used. By utilizing interferometric detection,[24, 25] the arrival time and therefore position inside the focus of a particular CARS feature can be found.

A diagram of such a system is outlined in Fig. 1. An illumination source that consists of a laser pulse or a pair of laser pulses is used as the pump and Stokes radiation to generate CARS. The illumination is shaped to stimulate a particular Raman resonance frequency of a target molecular species. The illumination is split into two by a beamsplitter to form an interferometer. The illumination in the sample arm of the interferometer is focused into the sample by a low NA objective. The beam will be scanned by either moving the beam or the sample so that transverse resolution can be obtained, while the axial resolution is given by the arrival time of the anti-Stokes. The backscattered anti-Stokes is collected from the sample and separated by a dichroic beamsplitter. In the reference arm, the illumination is focused into a sample with the same resonance frequency as the target species. The forward scattered light is collected and interferometrically cross-correlated with the light from the sample. This cross-correlation can be done in either the time domain or the frequency domain. The peaks of the cross-correlation will correspond to the anti-Stokes scatterers in the sample.

Note that backscattered CARS is employed, while phase matching favors forward scattering CARS in bulk materials. One way backscattering can occur is if the target species is present as randomly positioned subwavelength-sized particles. In this case, the phase matching condition of a bulk medium is relaxed and the CARS is emitted directly into the backscattered direction, producing epi-CARS.[26, 27] Another way backscatter-

ing can occur is if forward emitted CARS is subsequently linearly backscattered by another small particle within the focal volume. Because a nearby particle to a Raman scatterer is more likely to backscatter the anti-Stokes light than a far particle, we expect that the locality of the imaging will be preserved. It is likely that both of these mechanisms to contribute to the detected backscatterered CARS.

One disadvantage of not using tight focusing is that the incident intensity will be lower, and therefore less anti-Stokes light will be produced. For a constant incident average power, the the incident intensity will be proportional to the square of the NA (as NA^2). The generated anti-Stokes light varies as the cube of the incident intensity, which means that the total anti-Stokes radiation produced is proportional to NA^6. Therefore there is a significant penalty to be paid when using a low NA. This can be made up partially in two ways. Because the beam is illuminating a wider area, it is likely more average power can be used before tissue damage occurs by heating. In addition, a higher energy pulse can be used if it is stretched in time to keep the peak intensity low. Keeping the peak intensity low minimizes damage from multiphoton ionization and absorption, dielectric breakdown, and plasma formation. Therefore even μJ energy pulses may be employed if the peak power remains low.

In addition, a low numerical aperture also limits the amount of backscattered light that can be collected through the objective, because the objective will subtend a smaller solid angle relative to a scatterer. This will impose an additional NA^2 penalty on the amount of gathered backscattered anti-Stokes. This is compensated for by the fact that the area illuminated at the focus is proportional to NA^{-2}, making the collectable anti-Stokes vary as NA^6. This should be compared with standard OCT, which has a NA^2 dependence because it does not rely on nonlinear backscattering.

A significant advantage of using low numerical aperture focusing is that an entire axial scan can be taken at once, in analogy to Spectral Domain Optical Coherence Tomography (SD-OCT). By using spectral detection, the backscattered radiation generated by a single illumination pulse can be measured instantaneously. This can significantly speed up data acquisition because only one pulse need be used for each axial scan, in contrast to CARS microscopy which scans one point at a time. Therefore far fewer pulses are needed when a lower NA is used. By using fewer pulses, the individual pulse energy can be made greater while keeping average power low. This can help boost the instantaneous intensity to make up for the larger focal spot size. If a 1-kHz repetition rate mJ regenerative amplifier is used as the illumination source, 1000 axial scans can be taken per second, with each pulse being of μJ energy, but maintaining only mW of average power on the tissue.

The axial resolution of this method will depend, like standard OCT, on the bandwidth of the returned signal from the sample. It is desirable to maximize the bandwidth of the anti-Stokes light emitted to achieve the best range resolution. At the same time, we would like to only stimulate a single Raman resonance to be specific to a particular molecular species. This can be achieved by utilizing various broadband CARS excitation schemes, such as utilizing a pair of overlapped chirped pulses,[28] or applying a periodic perturbation to the pulse in the spectral domain.[29–32] Because these pulses are broadband the anti-Stokes radiation will be also, but the envelope of the pulse is shaped to only stimulate a particular Raman feature. These methods enable the pulse to be stretched out to minimize peak power but can excite a large Raman polarization. Another possibility is to use a pump/Stokes/probe combination where the pump and Stokes are narrowband to stimulate the Raman resonance, but the probe pulse is broadband to create a broad anti-Stokes spectrum. However, this presents the problem of obtaining synchronized broadband and narrowband pulses.

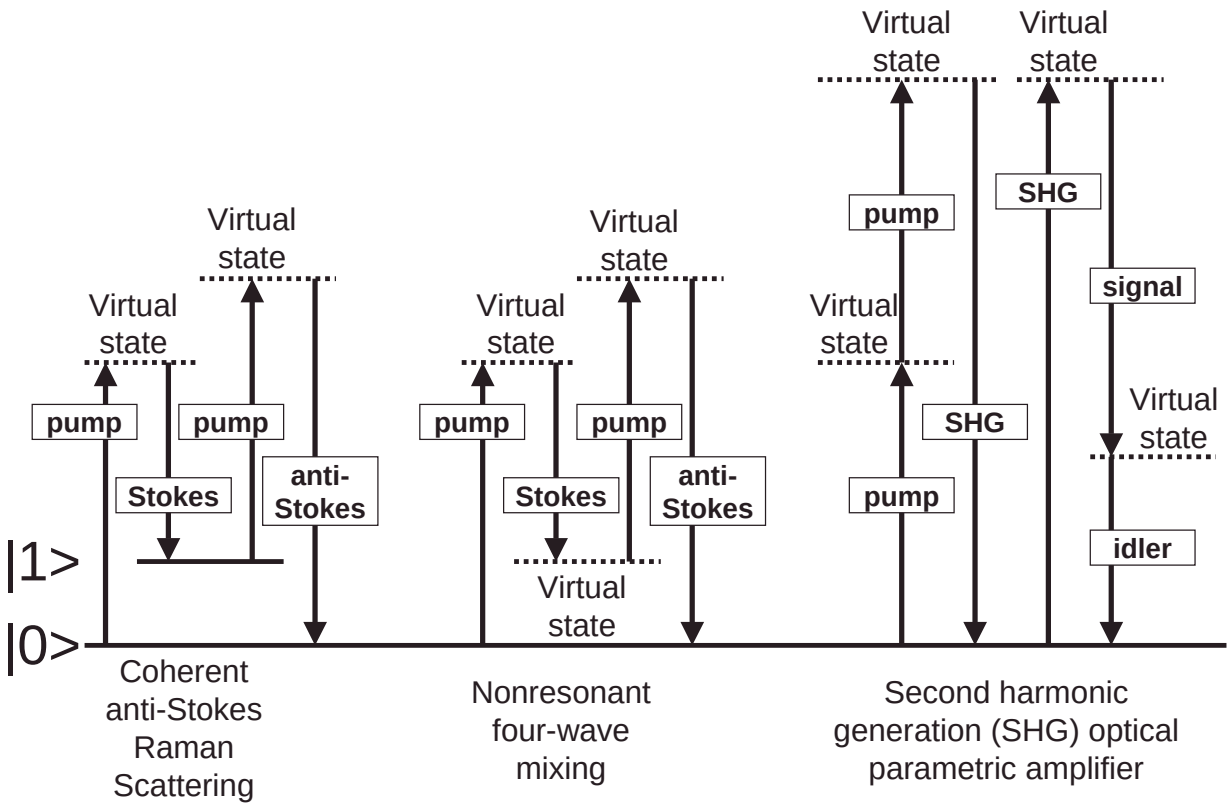

Figure 2. Diagram of four-wave-mixing processes utilized for CARS (left), nonresonant four-wave-mixing (middle), and the four-wave-mixing process mediated by two three-wave-mixing processes in a second-harmonic-generation optical-parametric-amplfiier.

2. APPROACH

Our approach is different than the method outlined above in that it generates the reference pulse in an alternate way. Because this is a hetetrodyne method, a reference pulse must be generated with a frequency identical to the CARS returning from the sample. This may be achieved in other ways than using an identical sample in the reference arm. To generate a Stokes pulse, we used a second-harmonic optical parameteric oscillator (SHG-OPA), which converts the second-harmonic of the pump pulse to signal and idler pulses. This process is illustrated in Fig. 2. The SHG-OPA consists of two three-wave-mixing processes that is equivalent to a single four-wave-mixing process. The SHG-OPA is used to generate an idler pulse that acts as the Stokes pulse that in combination with the pump pulse stimulates CARS in the sample. At the same time, the signal pulse generated by the SHG-OPA is the same frequency as the anti-Stokes created by the sample. Therefore the signal from the SHG-OPA can be used as a reference pulse to demodulate the anti-Stokes signal. Therefore the SHG-OPA is a convenient way to create a Stokes pulse and a reference pulse at the same time that are automatically matched, since the SHG-OPA and CARS are both four-wave-mixing processes.

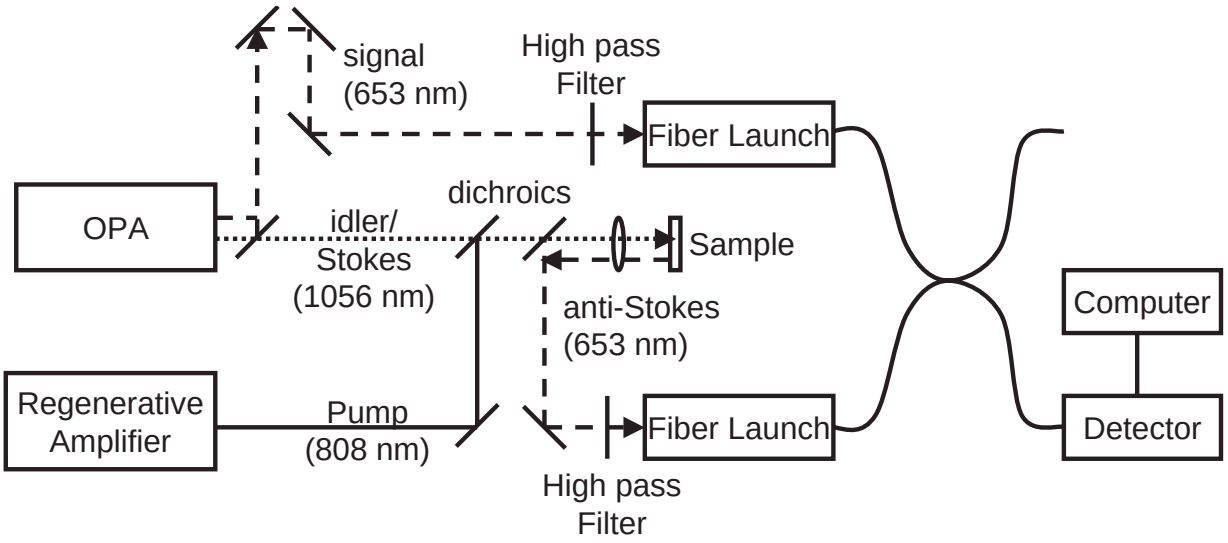

Figure 3. Schematic diagram of setup to measure CARS interferograms to range interfaces.

The setup used to acquire the CARS ranging is shown in Fig. 3 and is similar to that of Fig. 1. A regenerative amplifier (RegA 9000, Coherent Inc., Santa Clara, CA) produces pulses at 808 nm center wavelength, 30 nm bandwidth, and 250 kHz repetition rate with 1.35 W average output power. About 100 mW is used as a pump for CARS, the remainder pumps a SHG-OPA (OPA 9450, Coherent Inc., Santa Clara, CA). The OPA generates signal and idler pulses. The idler acts as a Stokes and is combined with the pump pulse which arrives at the same time at a dichroic beamsplitter. The pump and Stokes are focused into a sample by a low numerical aperture lens of 30 mm focal length and the backscattered anti-Stokes is collected. The anti-Stokes is separated by a dichroic beamsplitter, and is coupled into a 2x2 fiber beamsplitter coupler port after the remainder of the pump/Stokes is filtered out. At the same time, the signal from the OPA, which is the reference pulse, is delayed and then focused into the other port of the fiber beamsplitter. The interference is collected at one port at an avalanche photodiode. A mirror on a translation stage scans the delay. The interferogram is measured by sampling the photodiode current as the delay is scanned.

The sample imaged consists of two microscope slides with coverslips of approximately 120 μm thickness with a 100 μm spacer between the coverslip and slide, with a well for liquid inside the spacer. The slides are placed with the coverslip sides facing each other. The wells beneath the coverslips are filled with acetone, which has a C–H stretch vibration mode with is Raman-active at 2925 cm^{-1}. The OPA is tuned such that the difference between the pump and Stokes frequencies corresponds to the resonance frequency.

Figure 4 shows two demodulated interferograms measured by standard OCT and the anti-Stokes from the CARS ranging. The standard OCT is not molecularly sensitive, so it produces a reflection for all interfaces. On the left is a diagram of the two slides, with each interface between different materials marked with a boxed uppercase letter. The reflections in the OCT interferogram (a) are marked by the corresponding letters. Because OCT is not molecularly sensitive, each interface produces a reflection regardless of its composition. The CARS ranging interferogram (b) contains only two reflections corresponding to each acetone layer, which are also

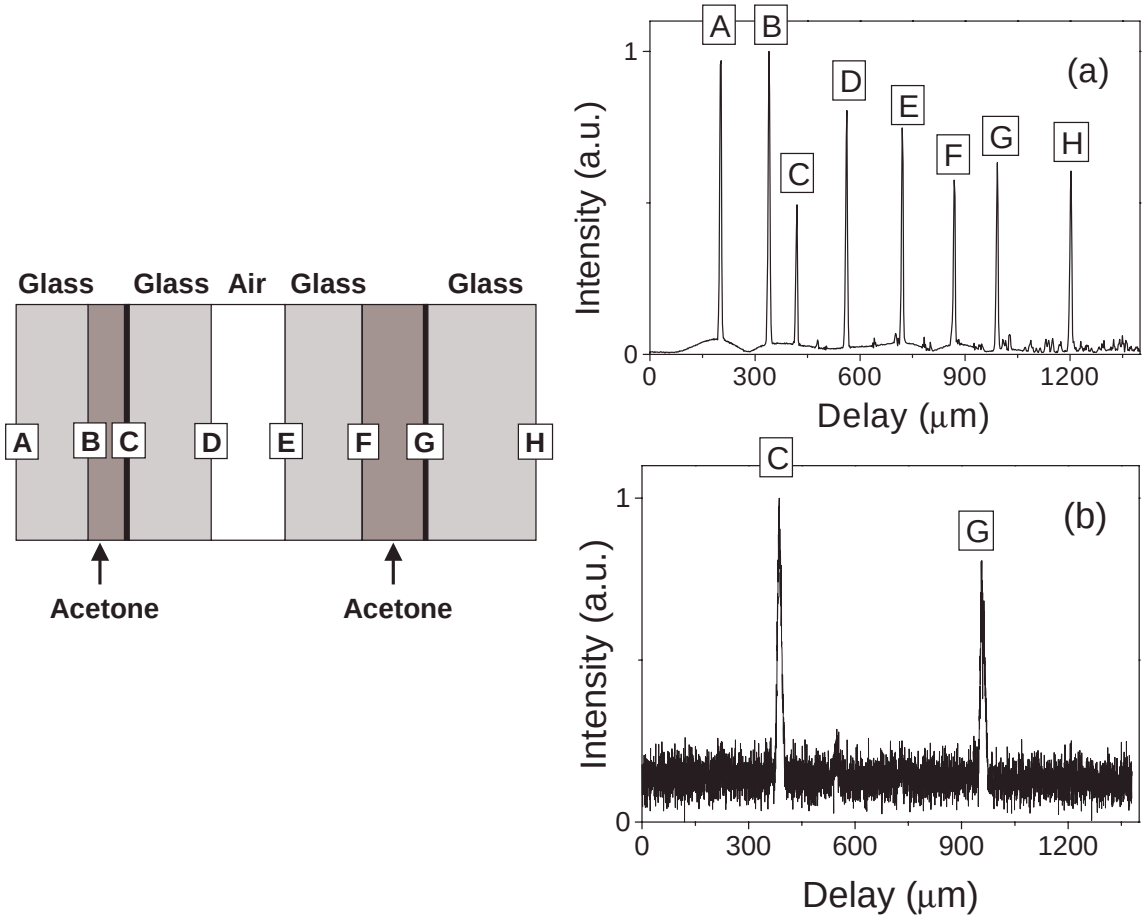

Figure 4. Demodulated interferograms of two slides measured by standard OCT (a) and CARS ranging (b). At the left is a diagram of the slides, with coverslips facing each other and acetone under the coverslips. Each interface is labeled with a boxed uppercase letter. In the OCT image (a), one can observe a reflection for each interface, which we have labeled with the corresponding letter. In the CARS ranging image (b), there are only two reflections due to the acetone regions.

marked with their respective letters. The positions of these reflections corresponds to the same interface in the OCT interferogram. These methods demonstrate that optical ranging of the CARS signal can be performed using methods common in OCT, which we call Nonlinear Interferometric Vibrational Imaging (NIVI). Molecular OCT imaging can be performed with the molecular sensitivity inherent to CARS, and without the limitations associated with the use of high numerical aperture objectives.

ACKNOWLEDGMENTS

We acknowledge the National Aeronautics and Space Administration and the National Institutes of Health (National Cancer Institute) for their support under grant number NAS2-02057.

REFERENCES

1. D. Huang, E. A. Swanson, C. P. Lin, J. S. Schuman, W. G. Stinson, W. Chang, M. R. Hee, T. Flotte, K. Gregory, C. A. Puliafito, and J. G. Fujimoto, "Optical Coherence Tomography," *Science* **254**(5035), pp. 1178–1181, 1991.
2. S. A. Boppart, G. J. Tearney, B. E. Bouma, J. F. Southern, M. E. Brezinski, and J. G. Fujimoto, "Noninvasive assessment of the developing Xenopus cardiovascular system using optical coherence tomography," *Proc. Natl. Acad. Sci. USA* **94**, pp. 4256–4261, 1997.
3. S. A. Boppart, B. E. Bouma, C. Pitris, J. F. Southern, M. E. Brezinski, and J. G. Fujimoto, "In vivo cellular optical coherence tomography imaging," *Nature Medicine* **4**, pp. 861–864, 1998.
4. J. G. Fujimoto, S. A. Pitris, S. A. Boppart, and M. E. Brezinski, "Optical coherence tomography: an emerging technology for biomedical imaging and optical biopsy," *Neoplasia* **2**, pp. 9–25, 2000.
5. J. M. Schmitt, S. H. Xiang, and K. M. Yang, "Differential absorption imaging with optical coherence tomography," *J. Opt. Soc. Am. A* **15**, pp. 2288–2296, 1998.
6. U. Morgner, W. Drexler, F. X. Kartner, X. D. Li, C. Pitris, E. P. Ippen, and J. G. Fujimoto, "Spectroscopic optical coherence tomography," *Opt. Lett.* **25**, pp. 111–113, 2000.
7. R. Leitgeb, M. Wojtkowski, A. Kowalczyk, C. K. Hitzenberger, M. Sticker, and A. F. Fercher, "Spectral measurement of absorption by spectroscopic frequency-domain optical coherence tomography," *Opt. Lett.* **25**, pp. 820–822, 2000.
8. G. J. Tearney, M. E. Brezinski, J. F. Southern, B. E. Bouma, M. R. Hee, and J. G. Fujimoto, "Determination of the refractive index of highly scattering human tissue by optical coherence tomography," *Opt. Lett.* **20**, pp. 2258–2260, 1995.
9. A. M. Zysk, J. J. Reynolds, D. L. Marks, P. S. Carney, and S. A. Boppart, "Projected index computed tomography," *Opt. Lett.* **28**, pp. 701–703, 2003.
10. J. F. de Boer, T. E. Milner, M. J. C. van Germert, and J. S. Nelson, "Two-dimensional birefringence imaging in biological tissue by polarization sensitive optical coherence tomography," *Opt. Lett.* **22**, pp. 934–936, 1997.
11. C. K. Hitzenberger, E. Gotzinger, M. Sticker, M. Pircher, and A. F. Fercher, "Measurement and imaging of birefringence and optic axis orientation by phase resolved polarization sensitive optical coherence tomography," *Opt. Expr.* **9**, pp. 780–790, 2001.
12. S. Jiao and L. V. Wang, "Two-dimensional depth-resolved Mueller matrix of biological tissue measured with double-beam polarization sensitive optical coherence tomography," *Opt. Lett.* **27**, pp. 101–103, 2002.

13. B. H. Park, C. Saxer, S. M. Srinivas, J. S. Nelson, and J. F. de Boer, "In vivo burn depth determination by high-speed fiber-based polarization sensitive optical coherence tomography," *J. Biomed. Opt.* **6**, pp. 474–479, 2001.
14. R. K. Kang, X. Xu, V. V. Tuchin, and J. B. Elder, "Concurrent enhancement of imaging depth contrast for optical coherence tomography by hyperosmotic agents," *J. Opt. Soc. Am. B* **18**, pp. 948–953, 2001.
15. T. M. Lee, A. L. Oldenburg, S. Sitafalwalla, D. L. Marks, W. Luo, F. J.-J. Toublan, K. S. Suslick, and S. A. Boppart, "Engineered microsphere contrast agents for optical coherence tomography," *Opt. Lett.* **28**, pp. 1546–1548, 2003.
16. M. D. Duncan, J. Reintjes, and T. J. Manuccia, "Scanning coherent anti-Stokes Raman microscope," *Opt. Lett.* **7**(8), pp. 350–352, 1982.
17. A. Zumbusch, G. R. Holtom, and X. S. Xie, "Three-dimensional vibrational imaging by Coherent Anti-Stokes Raman Scattering," *Phys. Rev. Lett.* **82**(20), pp. 4142–4145, 1999.
18. G. W. H. Wurpel, J. M. Schins, and M. Muller, "Direct measurement of chain order in single phospholipid mono- and bilayers with multiplex cars," *J. Phys. Chem. B* **108**, pp. 3400–3403, 2004.
19. K. P. Knutsen, J. C. Johnson, A. E. Miller, P. B. Petersen, and R. J. Saykally, "High spectral resolution multiplex CARS microscopy using chirped pulses," *Chem. Phys. Lett.* **387**, pp. 436–441, 2004.
20. E. O. Potma, D. J. Jones, J.-X. Cheng, X. S. Xie, and J. Ye, "High-sensitivity coherent anti-Stokes Raman scattering microscopy with two tightly synchronized picosecond lasers," *Opt. Lett.* **27**, pp. 1168–1170, 2002.
21. J.-X. Cheng, Y. K. Jia, G. Zheng, and X. S. Xie, "Laser-scanning coherent anti-Stokes Raman scattering microscopy and applications of cell biology," *Biophys. J.* **83**, pp. 502–509, 2002.
22. N. Dudovich, D. Oron, and Y. Silberberg, "Single-pulse coherent controlled nonlinear Raman spectroscopy and microscopy," *Nature* **418**, pp. 512–514, 2002.
23. N. Dudovich, D. Oron, and Y. Silberberg, "Single-pulse coherent anti-Stokes Raman spectroscopy in the fingerprint spectral region," *J. of Chem. Phys.* **118**(20), pp. 9208–9215, 2003.
24. D. L. Marks and S. A. Boppart, "Nonlinear interferometric vibrational imaging," *Phys. Rev. Lett.* **92**(12), pp. 123905–1–123905–4, 2004.
25. C. Vinegoni, J. S. Bredfeldt, D. L. Marks, and S. A. Boppart, "Nonlinear optical contrast enhancement for optical coherence tomography," *Opt. Expr.* **12**(2), pp. 331–341, 2004.
26. J.-X. Cheng, A. Volkmer, L. D. Book, and X. S. Xie, "An Epi-Detected Anti-Stokes Raman Scattering (E-CARS) Microscope with High Spectral Resolution and High Sensitivity," *J. of Phys. Chem. B* **105**, pp. 1277–1280, 2001.
27. A. Volkmer, J.-X. Cheng, and X. S. Xie, "Vibrational imaging with high sensitivity via epidetected coherent anti-Stokes Raman scattering microscopy," *Phys. Rev. Lett.* **87**(2), pp. 023901–1–023901–4, 2001.
28. E. Gershgoren, R. A. Bartels, J. T. Fourkas, R. Tobey, M. M. Murnane, and H. C. Kapteyn, "Simplified setup for high-resolution spectroscopy that uses ultrashort pulses," *Opt. Lett.* **28**(5), pp. 361–363, 2003.
29. A. M. Weiner, D. E. Leaird, G. P. Wiederrech, and K. A. Nelson, "Femtosecond pulse sequences used for optical manipulation of molecular motion," *Science* **247**(4948), pp. 1317–1319, 1990.
30. D. Oron, N. Dudovich, D. Yelin, and Y. Silberberg, "Narrow-band coherent anti-Stokes Raman signals from broad-band pulses," *Phys. Rev. Lett.* **88**(6), pp. 063004–1–063004–4, 2002.
31. D. Oron, N. Dudovich, D. Yelin, and Y. Silberberg, "Quantum control of coherent anti-Stokes Raman processes," *Phys. Rev. A* **65**, pp. 043408–1–043408–4, 2002.
32. D. Oron, N. Dudovich, and Y. Silberberg, "Femtosecond phase-and-polarization control for background-free coherent anti-Stokes Raman spectroscopy," *Phys. Rev. Lett.* **90**(21), pp. 213902–1–213902–4, 2002.